



# Unraveling Metal-insulator Transition Mechanism of VO<sub>2</sub> Triggered by Tungsten Doping

Xiaogang Tan<sup>1\*</sup>, Tao Yao<sup>2\*</sup>, Ran Long<sup>1</sup>, Zhihu Sun<sup>2</sup>, Yajuan Feng<sup>2</sup>, Hao Cheng<sup>2</sup>, Xun Yuan<sup>3</sup>, Wenqing Zhang<sup>3</sup>, Qinghua Liu<sup>2</sup>, Changzheng Wu<sup>1</sup>, Yi Xie<sup>1</sup> & Shiqiang Wei<sup>2</sup>

<sup>1</sup>Hefei National Laboratory for Physical Sciences at Microscale, University of Science and Technology of China, Hefei 230026, China, <sup>2</sup>National Synchrotron Radiation Laboratory, University of Science and Technology of China, Hefei, 230029, China, <sup>3</sup>State Key Laboratory of High Performance Ceramics and Superfine Microstructures, Shanghai Institute of Ceramics, Chinese Academy of Sciences, Shanghai 200050, China.

Received  
30 March 2012

Accepted  
8 June 2012

Published  
22 June 2012

Correspondence and requests for materials should be addressed to Y.X. (yxie@ustc.edu.cn) or S.Q.W. (sqwei@ustc.edu.cn).

\* These authors contributed equally to this work.

Understanding the mechanism of W-doping induced reduction of critical temperature ( $T_C$ ) for VO<sub>2</sub> metal-insulator transition (MIT) is crucial for both fundamental study and technological application. Here, using synchrotron radiation X-ray absorption spectroscopy combined with first-principles calculations, we unveil the atomic structure evolutions of W dopant and its role in tailoring the  $T_C$  of VO<sub>2</sub> MIT. We find that the local structure around W atom is intrinsically symmetric with a tetragonal-like structure, exhibiting a concentration-dependent evolution involving the initial distortion, further repulsion, and final stabilization due to the strong interaction between doped W atoms and VO<sub>2</sub> lattices across the MIT. These results directly give the experimental evidence that the symmetric W core drives the detwisting of the nearby asymmetric monoclinic VO<sub>2</sub> lattice to form rutile-like VO<sub>2</sub> nuclei, and the propagations of these W-encapsulated nuclei through the matrix lower the thermal energy barrier for phase transition.

Monoclinic/rutile vanadium dioxide VO<sub>2</sub> (M1/R), a model metal-insulator transition (MIT) material, displays a first-order transition from a monoclinic insulating phase to a tetragonal metallic phase at a critical temperature ( $T_C$ ) of 341 K, accompanied by a reversible switch in optical transmittance/reflectance in the infrared range<sup>1</sup>. This dramatic phase transition makes VO<sub>2</sub> potentially useful for 'smart' optical and electrical switches, which yet requires the regulation of  $T_C$  to around room temperature (RT)<sup>2-6</sup>. The most effective route for appreciable reduction of  $T_C$  is doping some donor impurity atoms, which could be easily realized by chemical substitution methods<sup>7-10</sup>. In particular, doping the V sublattice with W is very attractive since it yields a pronounced reduction in  $T_C$  by ~20 K/at.%W for the bulk and by ~50 K/at.%W for the nanostructure, and even metallic ground state is realized for W concentration of  $\geq 8$  at.%<sup>7,8</sup>. Therefore, W-doped VO<sub>2</sub> system has been widely used as key building blocks for some smart devices, such as thermochromics and variable-reflectance mirrors<sup>8,9</sup>. However, there are still many intriguing questions to be resolved: why such a small amount of W dopant could introduce so large a reduction in  $T_C$  and what is the underlying physical mechanism to drive the MIT transition when W is involved? Right answers to these questions would enrich our understanding on the exact interplay of electron and lattice of correlated materials during MIT mechanism.

Several experimental investigations have been carried out on the W<sub>x</sub>V<sub>1-x</sub>O<sub>2</sub> systems and attempted to present some structural and mechanistic explanations<sup>10-12</sup>. By using small-angle X-ray scattering and X-ray absorption methods, Tang *et al.* considered that the charger transfer from W ions weakens the V-V pairs, promoting the structural transformation from monoclinic to rutile<sup>11</sup>. Also, Booth *et al.* found that a significant expansion in certain crystal axes induced by W dopants breaks the Peierls-paired V ions, leading to the reduction of  $T_C$ <sup>12</sup>. However, these studies are limited to heavily-doped samples with relatively lower  $T_C$ , in which the VO<sub>2</sub> host lattice is close to rutile phase at RT. As a result, only the final state affected by W doping is obtained, which can be found from their stable and almost invariable local structure (LS) around W atoms. On the other hand, the interatomic distances of W dopants are short in heavily-doped samples; therefore the strong coupling effect between the neighboring W atoms makes it difficult to isolate the structure and contribution of a single W atom from its environment. Therefore, the real W local structure and its effect on the surrounding monoclinic VO<sub>2</sub> matrix, as well as its evolutions during MIT remain obscure. In order to attain physical insights into W-induced  $T_C$  reduction, one promising way is to conduct detailed structural characterizations on specimen with wide



concentration gradients, which exhibits the reduction of  $T_C$  from several to dozens of degrees. For this purpose a rather suitable tool is X-ray absorption fine structure (XAFS) spectroscopy thanks to its element selectivity and good sensitivity to local structures<sup>13</sup>, which allows one to separately probe and compare the LS around V and W atoms in a same sample, even in the dilute doping case. In fact, the capability of XAFS has been demonstrated in a recent work that provides a very distinct, qualitative signature for the monoclinic-to-tetragonal transformation in  $\text{VO}_2$ <sup>14</sup>.

In this work, to completely understand the  $T_C$  reduction mechanism induced by W-doping, we study systematically the LS around W and V atoms in single crystals  $\text{W}_x\text{V}_{1-x}\text{O}_2$  with a wide doping range from dilute to heavy concentrations ( $x = 0.54\%$ ,  $0.95\%$ ,  $1.45\%$  and  $2.38\%$ ) using the XAFS technique. These representative concentrations allow us to present for the first time: (i) a clear figure of LS around an isolated W dopant in the monoclinic  $\text{VO}_2$  lattice, and (ii) the reconstruction of concentration-dependent evolutions of W and V structures across the  $\text{VO}_2$  MIT.

## Results

The  $T_C$  and the crystalline structures for the  $\text{W}_x\text{V}_{1-x}\text{O}_2$  samples are determined by DSC and XRD as shown in Figure 1. DSC analysis indicates that increasing W content  $x$  from  $0.54\%$  to  $2.38\%$  significantly reduces  $T_C$  from  $54.1$  to  $-50^\circ\text{C}$  (Figure 1a). The plot of  $T_C$  as a function of W concentration in Figure 1b shows an approximate linear relation with a slope of  $\sim 20$  K/at.%W, comparable with that  $\sim 22$  K/at. %W for thin films reported previously<sup>7</sup>. The RT XRD patterns displayed in Figure 1c exhibit two characteristic diffraction peaks (asterisks) assignable to the monoclinic phase for the  $x = 0.54\%$  sample, suggesting the primary monoclinic  $\text{VO}_2$  structure. At higher doping level ( $x \geq 1.45\%$ ), only the diffraction peaks corresponding to tetragonal phase can be observed<sup>15</sup>, demonstrating the complete transformation into rutile phase of  $\text{VO}_2$ . It should be noted that

the magnitude of the phase transition is weakened with increasing W concentration, reflected by the peaks in DSC results, the phenomenon of which is well known in heavy atoms (W, or Mo) doped  $\text{VO}_2$ <sup>7,16</sup>. Although it is truly a practical problem, the W-doping is known as the most effective route to reduce  $T_C$ , and has been considered as the prototypical model in understanding the mechanism by which the  $T_C$  of  $\text{VO}_2$  MIT could be manipulated.

To obtain detailed structural information, we performed element-specific XAFS measurements on both host V and doped W atoms. Figures 2(a) and 2(b) show the V  $K$ -edge extended XAFS (EXAFS) oscillation  $\chi(k)$  functions and their Fourier transforms (FTs), respectively, along with the calculated EXAFS data for  $\text{VO}_2$  with monoclinic (M1, space group P21/c), rutile (R, space group P42/mnm) and another monoclinic (M2, space group C2/m) phases as the references. With increasing W content, the LS around V atoms gradually evolve into that in tetragonal phase, as indicated by the featured changes in the  $k$  range of  $4\text{--}8 \text{ \AA}^{-1}$  (Figure 2a)<sup>14</sup>. Correlated changes can be identified in FTs profiles (Figure 2b). The  $\text{VO}_2$  lattice structure of  $0.54\%$  W doped sample remains in the monoclinic phase, because its FTs curve keeps the main features with that of pure monoclinic phase. When W content increases to  $0.95\%$ , the two V-O split peaks merge into a single peak at  $1.48 \text{ \AA}$  and the V-V1 peak at  $2.12 \text{ \AA}$  disappear, implying that the initial monoclinic  $\text{VO}_2$  phase has been largely distorted towards tetragonal phase at RT. For the  $1.45\%$  and  $2.38\%$  W doped samples, the FTs curves match well with that of calculated tetragonal  $\text{VO}_2$  phase. The structural transition from monoclinic to tetragonal phase with increasing W concentration clearly confirms the reduction of  $T_C$ , consistent with the XRD and DSC results.

Of note, the formation of the metastable M2 phase that has partial dimerization of the V-V chains was reported in the monoclinic to rutile phase transformation<sup>10,15,17–21</sup>. However, metastable M2 phase is indeed tightly associated with the strains, and are nearly all found

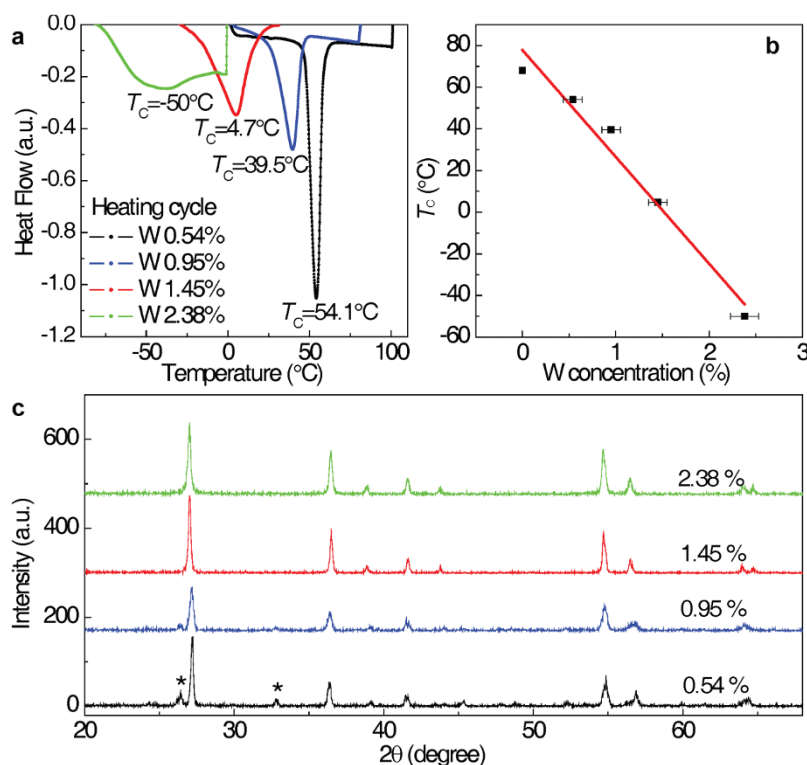


**Figure 1** | The  $T_C$  and the overall structures for the prepared samples  $\text{W}_x\text{V}_{1-x}\text{O}_2$ . (a) The DSC measurement results for samples with different W doping concentration. (b) The plot of transition temperature  $T_C$  as function of W composition  $x$  for  $\text{W}_x\text{V}_{1-x}\text{O}_2$  single crystals.  $T_C$  values are effectively reduced by W doping at  $\sim 20$  K/at.% W. (c) The XRD patterns measured at room temperature for  $\text{W}_x\text{V}_{1-x}\text{O}_2$  samples. The diffraction peaks correspond to the rutile phase, while the additional peaks (indicated by asterisks) correspond to the monoclinic phase.

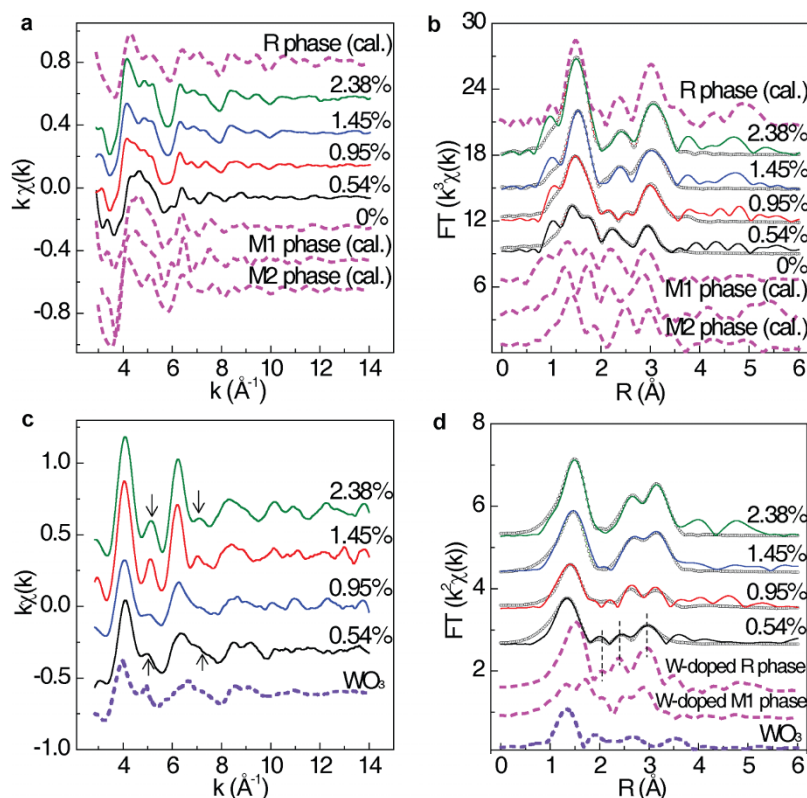


**Figure 2** | XAFS results for  $W_xV_{1-x}O_2$ . (a) The V  $K$ -edge EXAFS oscillations and (b) their Fourier transforms for  $W_xV_{1-x}O_2$  samples, along with the  $VO_2$  theoretical results of monoclinic (M1), rutile (R) and another monoclinic (M2) phases for references. (c) The W  $L_3$ -edge EXAFS oscillations and (d) their Fourier transforms, along with the reference  $WO_3$  result, and the simulated curves for W-substituted monoclinic and tetragonal  $VO_2$  phases. Fitting results are plotted as open circles.

within the nanostructures that have strong surface-induced stress to stabilize M2 phase<sup>10,15,17</sup>, while there is no evidence for isolation of stable M2 phase for large  $VO_2$  crystallites without apparent stresses and defects<sup>18</sup>. Even in doped bulk  $VO_2$  crystallites, only the Al and Cr doping that could result in the increase of  $T_C$  are reported to stabilize the M2 phase<sup>19,20</sup>. Compared with W ions, these dopants have smaller ionic radii and are acceptor impurities, which would lead to the differentiation of two types of V atoms, corresponding to the proposed M2 monoclinic phase<sup>21</sup>. Hence, we consider that the intermediate M2 phase can be precluded in our highly crystalline W-doped  $VO_2$ , in agreement with the previous reports<sup>12,22</sup>. This conclusion can be further confirmed by the significant differences in the oscillation  $\chi(k)$  and FT curve between the calculated spectrum of M2 structure and our samples.

We further focus on the LS around W atoms that could be deduced from W  $L_3$ -edge XAFS data (Figures 2c and 2d). The LS around W atom should be symmetric in nature similar to the reference  $WO_3$ . This is inferred from the fact that these samples, like  $WO_3$ , also present two peaks at 4.0 and 6.2  $\text{\AA}^{-1}$  in the low  $k$  region (3–8  $\text{\AA}^{-1}$ ) of the  $k\chi(k)$  oscillation curves (Figure 2c), and only one prominent W–O peak without splitting appears in the FTs curves (Figure 2d). It should also be noted that the symmetry around W core at the low concentration ( $< 1\%$ ) is distorted due to the significant compression of almost isolated W dopants by the overwhelmingly asymmetric monoclinic  $VO_2$  lattices, which can be reflected by the missed fine features (marked by arrows) in the 3–8  $\text{\AA}^{-1}$  region, as well as by the damped oscillations in the 8–14  $\text{\AA}^{-1}$  region. Furthermore, we have also calculated the W  $L_3$ -edge FTs spectra for the W-substituted monoclinic and tetragonal  $VO_2$  phases. Interestingly, the FT curve of low-doped (0.54%) sample is more similar to the calculated spectrum of the W-substituted tetragonal phase than that of

W-substituted monoclinic phase which shows an obvious splitting for W–O peaks. Only a slight difference can be found for the position of W–O peaks which shifts from 1.35  $\text{\AA}$  of  $WO_3$  toward 1.51  $\text{\AA}$  of W-substituted tetragonal phase with increasing W concentration. Although the host  $VO_2$  is in monoclinic structure inferred by XRD results, the local environment of W dopant in the monoclinic  $VO_2$  matrix has yet assembled the tetragonal-like structure with compressed W–O pairs, implying the W-doping induced structural transition of the neighboring host  $VO_2$  lattice. Increasing  $x$ , the W–V1 and W–V2 peak positions (2.42 and 2.97  $\text{\AA}$ , respectively) increase to 2.67  $\text{\AA}$  and 3.13  $\text{\AA}$ , respectively, along with the enhancement of their intensities, implying the expansion of W local structures. The FT curves for highly doped samples ( $x \geq 0.95\%$ ), particularly the W–V peaks, are almost independent of the W concentration, and this trend continues until the heavy doping level of  $5\% \leq x \leq 33\%$  as reported in Ref. 11. These indicate that the LS around W atoms would not undergo remarkable changes when the  $VO_2$  host lattice is already in or near the rutile phase if the W concentration reaches a certain level, confirming the intrinsic and stable nature of symmetric W structure.

The quantitative structural information was extracted from EXAFS data fitting using the ARTEMIS module of IFEFFIT. The extracted parameters are summarized in Figure 3 and Table I and II. The obtained V–O and V–V distances show that the monoclinic  $VO_2$  host lattice is largely distorted in the  $x=0.95\%$  sample, and has completely transformed into tetragonal rutile structure when  $x$  increases to 1.45%. Because of the slight distortion of W atoms by the surrounding  $VO_2$  lattice, the EXAFS data for  $x=0.54\%$  sample were fitted using the monoclinic phase with degenerate W–O bonds. The rest three can be fitted well by using tetragonal rutile phase, due to their higher symmetric structures. The trend in Figure 2b shows

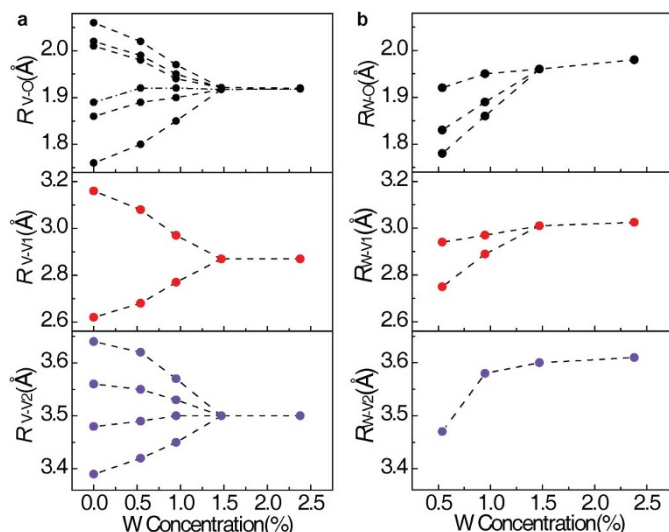


**Figure 3 | The bond distances as a function of W concentration.** The bond distances of the nearest three shells of (a) V and (b) W as the center atom, based on the XAFS fitting results of each sample with different W doping concentration.

steady increase of the average W–O and W–V bond distances, confirming the gradual expansion and relaxation of LS around W atoms with increasing W content. Here, we have found the expansion of both W–O and W–V1 pairs, which however are shown constant in Ref. 12, with the W concentration. The whole expansion observed here can be ascribed to the distinct W concentration gradient, thus reflecting the real evolution of LS of W dopants in monoclinic VO<sub>2</sub> across MIT.

## Discussion

Summarizing our experimental results, we schematically show in Figures 4a–c the crystal structure variations for W-doped VO<sub>2</sub> samples with three representative concentrations (0.54%, 0.95% and 2.38%). For the purpose of clarity, we magnify the structural model around W atoms in a planar visual. At first sight, the LS around W atom highlighted in white exhibits two prominent features: the increased symmetry and the expanded volume. A point worth emphasizing is that several XAFS studies by Patridge *et al.*<sup>23</sup>, Booth *et al.*<sup>12</sup>, and Whittaker *et al.*<sup>10</sup>, as well as the static lattice calculations by Netsianda *et al.*<sup>24</sup>, had suggested that dopants induce a local structural distortion towards high symmetry of rutile phase, which is generally accepted in the work of doping-induced phase transition of VO<sub>2</sub>. Moreover, our results not only confirm this basic model, but also demonstrate a concentration-dependent evolution of LS of W atoms. We find that the LS of W atom at low concentration is tetragonal-like but distorted by surrounding asymmetric monoclinic VO<sub>2</sub> lattice; at high doping level, the repulsion of these distorted

tetragonal units drives them to restore and stabilize the symmetric structure. This structural evolution of W atoms reflects the strong interaction between W and VO<sub>2</sub> structures that triggers the structural derivations of near VO<sub>2</sub> lattice from asymmetric monoclinic phase towards more symmetric.

To reveal the reason why a small amount of W doping lowers the T<sub>C</sub>, we performed density functional theory (DFT) calculations with Vienna Ab-initio Simulation Package (VASP) code based on the atomic structural parameters by XAFS. The calculations employed the projector augmented wave (PAW) method and the generalized gradient approximation (PBE-GGA) for electron exchange–correlation interaction<sup>25,26</sup>. A super large 4×3×5 supercell with 432 atoms containing 143 V atoms, 288 O atoms and 1 W atom, corresponding to ~0.6 % W concentration was used. At this concentration, the VO<sub>2</sub> lattice is of the monoclinic structure in the temperature range from 0 K to RT. We first considered the spatial extension of the influence on the atomic and electronic structures of VO<sub>2</sub> by W doping. Figure 4d shows the relaxed structure projected along [010], in which the distortion degree of VO<sub>2</sub> lattice is characterized by the difference of bond length  $|\Delta R|$  ( $|\Delta R| = |R_{\text{distorted}} - R_{\text{previous}}|$ ). We can find that the structural change shows a dopant-centred nature, since  $|\Delta R|$  near W dopants are all larger than 0.01 Å whereas those far away from W atoms are  $\leq 0.002$  Å. Furthermore, we examine the spatial redistribution of charge density upon doping W ions (Figure 4e). Also, the electron density pile-up is only significant in the neighborhood of W atoms along or cross the *c* axis. This is reasonable because the VO<sub>2</sub> structures away from W atoms remain in the insulating monoclinic phase which inhibits electron mobility<sup>27</sup>. Importantly, the relaxed structures in the theoretic calculations confirm that W dopants could induce large variations in both atomic and electronic structures of nearby VO<sub>2</sub> lattice. In this sense, the incorporation of local lattice disorder induced by the insert of W ions with larger volume, and the pile-up of itinerant electrons on the neighboring V-sites released by W ions with higher valence suppress the dimerized lattice distortion and destabilize insulating phase of VO<sub>2</sub>.

On the basis of experimental and theoretical results, we consider that the W-doping effect is confined in a local area (covered by each blue area of W cores schematically illustrated in Figure 4f), in which the VO<sub>2</sub> has accomplished the phase transition, and can be seen as the nucleus for MIT. Due to the existences of these pre-MIT nuclei, the thermal energy needed to trigger MIT is lowered compared with that for pure VO<sub>2</sub> single crystals<sup>28,29</sup>. At the low doping concentration, the nucleus can be seen as isolated, while at higher concentration two neighboring nuclei could touch each other due to the increased average W–W distance (the overlapped area shown in Figure 4f). Meanwhile, the XAFS results of the steady expansion of W structures and significant phase transition of VO<sub>2</sub> lattices suggested the propagation of W-induced changes towards the farther V atoms. Therefore, the increased formation of nuclei, along with their percolation in the materials, will further lowers thermal energy to fulfill the whole phase transition as expected. This picture of concentration scaled influence of W dopants is somewhat like the “metallic nanopuddles” in thermal-induced pure VO<sub>2</sub> MIT process<sup>30</sup>, in which

**Table 1 | EXAFS fitting results deduced from V Kedge spectra of W<sub>x</sub>V<sub>1-x</sub>O<sub>2</sub> samples**

W %	R-factor	V–O (Å) (±0.02)	$\sigma^2$ (10 <sup>-3</sup> Å <sup>2</sup> )	V–V (Å) (±0.02)	$\sigma^2$ (10 <sup>-3</sup> Å <sup>2</sup> )	$\Delta E_0$ (eV)
0.54	0.029	1.80/1.89/1.92	3.1 (±0.3)	2.68/3.08	2.9 (±1.7)	3.7 (±1.6)
		1.98/1.99/2.02	4.0 (±1.1)	3.42/3.49/3.55/3.62	4.0 (±2.1)	
0.95	0.038	1.85/1.90/1.92	2.8 (±2.0)	2.77/2.97	3.7 (±2.3)	–5.5 (±2.3)
		1.94/1.95/1.97	3.7 (±1.9)	3.45/3.50/3.53/3.57	5.8 (±1.6)	
1.54	0.032	1.92	8.2 (±3.5)	2.87	3.0 (±1.8)	–3.1 (±2.6)
				3.50	4.5 (±2.5)	
2.38	0.027	1.92	8.5 (±4.1)	2.87	2.8 (±1.9)	4.3 (±1.1)
				3.50	3.6 (±2.7)	



Table 2 | EXAFS fitting results deduced from W  $L_3$ -edge spectra of  $W_xV_{1-x}O_2$  samples

W%	R-factor	V-O (Å) ( $\pm 0.02$ )	$\sigma^2$ ( $10^{-3}$ Å <sup>2</sup> )	V-V (Å) ( $\pm 0.02$ )	$\sigma^2$ ( $10^{-3}$ Å <sup>2</sup> )	$\Delta E_0$ (eV)
0.54	0.049	1.78/1.83/1.92	5.1 ( $\pm 1.3$ )	2.75/2.94/3.47	9.2 ( $\pm 2.6$ )	-3.1 ( $\pm 1.6$ )
0.95	0.059	1.86/1.89/1.95	4.7 ( $\pm 3.0$ )	2.89/2.96/3.57	3.7 ( $\pm 2.3$ )	8.1 ( $\pm 1.7$ )
1.54	0.023	1.96	3.6 ( $\pm 1.3$ )	3.01/3.60	6.2 ( $\pm 2.1$ )	-2.1 ( $\pm 1.5$ )
2.38	0.028	1.98	3.2 ( $\pm 1.1$ )	3.10/3.63	5.6 ( $\pm 1.5$ )	-3.4 ( $\pm 0.8$ )

Qazilbash *et al.* have revealed that nanoscale percolative MIT took place first with metallic puddles in insulating host, and subsequent heating drives its complete transformation to metallic phase.

In conclusion, the behavior of an isolated W dopant and its influence on the  $VO_2$  host lattice are for the first time figured out by X-ray absorption spectroscopy coupled with the first-principle calculations, which helps us to unravel the mechanism of the reduction of MIT  $T_C$  induced by W-doping. A clear atomic structure of isolated W dopant has been unveiled, which possesses an intrinsically symmetric tetragonal-like structure, driving the detwisting of the nearby asymmetric monoclinic  $VO_2$  lattice towards rutile phase. These W-encapsulated rutile-like  $VO_2$  regions in fact act as nuclei for the “metallic puddles” which propagate through the host matrix, thus lowering the thermal activation energy across phase transition. These results also provide a clear indication to modulate the  $T_C$  by doping impurity with symmetry corresponding to that of targeted structure, which has been noticed in some syntheses.

## Methods

**Synthesis and Characterization.** Single crystals of  $W_xV_{1-x}O_2$  used in this study were prepared by reacting vanadyl acetylacetonate ( $VO(acac)_2$ ) with the required amount of sodium tungstate ( $Na_2WO_4$ ) in aqueous solution at 200 °C for 12 hours. The resultant products were calcined under argon at 700 °C for 8 hours. The phase homogeneity and the reversible transition characteristics of the samples were confirmed by X-ray diffraction (XRD) and differential scanning calorimetry (DSC). XAFS data at the W  $L_3$  and V  $K$ -edges were collected in fluorescence and transmission modes, respectively, at ambient temperature (25 °C) on beam lines U7B and U7C of the National Synchrotron Radiation Laboratory, China. The storage rings of NSRL were operated at 0.8 GeV with the maximum current of 200 mA. The hard x-ray beam was from a three-pole superconducting Wiggler with a magnetic field intensity of 6 T. The fixed-exit Si(111) flat double crystals were used as monochromator. Ionization chambers filled with Ar/ $N_2$ , and a 7-element pure Ge solid-state detector were used for the transmission and fluorescence x-ray detection, respectively.

**XAFS data analysis.** The EXAFS signals,  $\chi(k)$ , were extracted from the absorption raw data,  $\mu(E)$  from the averaged experimental spectra of four repeated scans, by using the ATHENA module<sup>31</sup> implemented in the IFEFFIT package<sup>32</sup> and the USTCXAFS software packages<sup>33</sup>. The  $\chi(k)$  data were weighted by  $k^3$  and  $k^2$  for V and

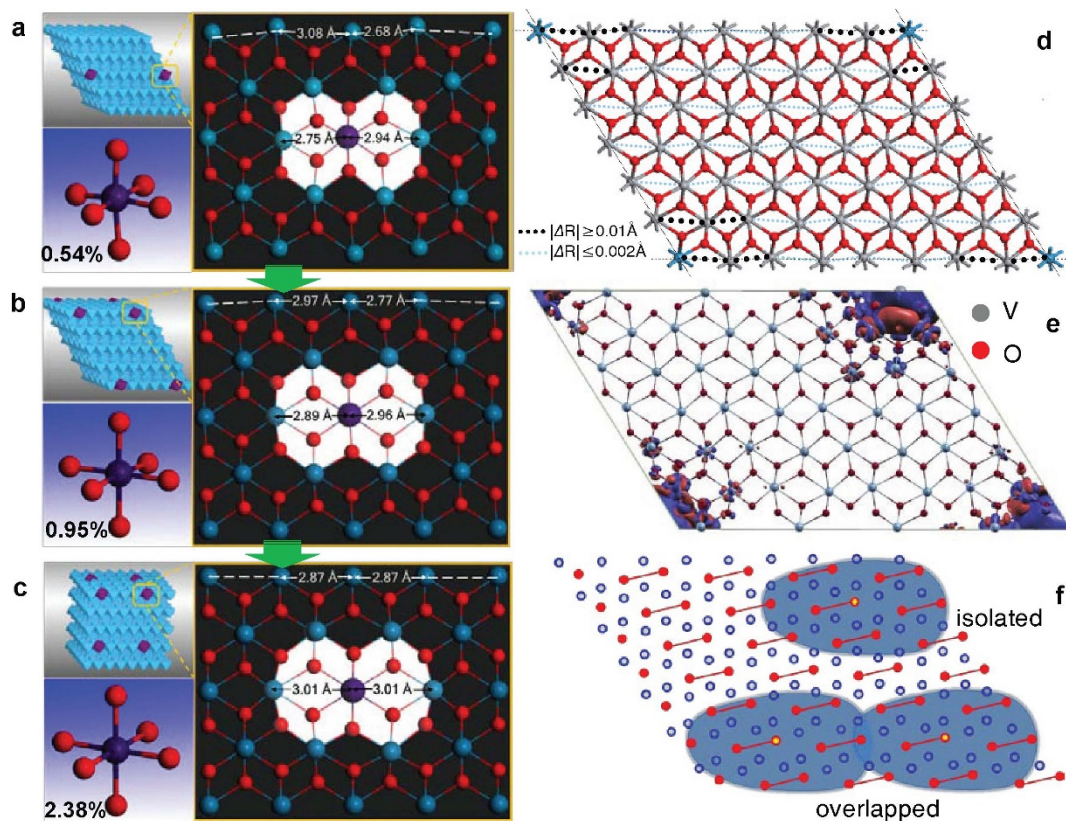


**Figure 4 | Models and theoretical calculations.** Models of LS distortions of three representative doped concentrations (a) 0.54%, (b) 0.95%, and (c) 2.38%. The white area displays the LS evolutions around W atoms. The variations of average W-W distances and  $[WO_6]$  octahedral geometries are shown in the left top and bottom panel, respectively. (d) The relaxed structure projected along  $[010]$  axis and (e) the corresponding spatial redistribution of charge density of W doped  $VO_2$  with about 0.6% concentration;  $|\Delta R|$  ( $|\Delta R| = |R_{\text{distorted}} - R_{\text{previous}}|$ ) based on calculation results give a distinct pattern of doped effects. The blue and red isosurfaces correspond to charge densities of  $0.005 \text{ e}/\text{\AA}^{-3}$  and  $-0.005 \text{ e}/\text{\AA}^{-3}$ , respectively. (f) A schematic diagram of concentration scaled influences of W dopants in  $VO_2$ , in which shows the low concentration with isolated dopants and the high concentration with interactional dopants.



W, respectively. The normalized absorption data were Fourier transformed using a  $k$ -space range of 2.8–14  $\text{\AA}^{-1}$ . The theoretical scattering amplitude and phase shift functions for all the paths were calculated by using the FEFF7 code. The  $V$   $K$ -edge XAFS spectra below and above 0.95% W concentration can be fitted well using the structural model of monoclinic  $\text{VO}_2$  (P21/c) and tetragonal  $\text{VO}_2$  (P42/mmm) based on ICSD #15889 and #4110, respectively. According to the  $T_C$ ,  $W$   $L_3$ -edge XAFS spectra below and above 0.95% concentration was fitted in the framework of monoclinic and tetragonal phase, respectively. The FEFF input files for the fitting of  $W$   $L_3$ -edge XAFS spectra was altered by replacing the  $V$  core in the monoclinic and tetragonal FEFF input files with  $W$ . The fitting was done in the  $R$  range [0.8, 3.8]  $\text{\AA}$  for all the data. In order to decrease the number of independent parameters, in the fitting procedure the coordination number was fixed to the nominal value for each scattering path, because the coordination numbers are not changed during MIT. For the monoclinic phase, the variation of  $M$ - $O$  ( $M=V$  and  $W$ ) bond distances in the range of 1.76–2.03  $\text{\AA}$  are classified into three groups, i.e., (1.76  $\text{\AA}$ ), (1.86  $\text{\AA}$ , 1.87  $\text{\AA}$ ), (2.00  $\text{\AA}$ , 2.01  $\text{\AA}$  and 2.04  $\text{\AA}$ ) according to their contribution to the scattering paths, and four kind  $M$ - $V_2$  bond distances (3.36  $\text{\AA}$ , 3.46  $\text{\AA}$ , 3.56  $\text{\AA}$  and 3.66  $\text{\AA}$ ) are included in the fitting. For each shell, the interatomic distance  $R$ , the Debye-Waller factor  $\sigma^2$ , and the edge-energy shift  $\Delta E_0$  were allowed to vary.

- Imada, M., Fujimori, A. & Tokura, Y. Metal-insulator transitions. *Rev. Mod. Phys.* **70**, 1039–1263 (1998).
- Cao, J. *et al.* Strain engineering and one-dimensional organization of metal-insulator domains in single-crystal vanadium dioxide beams. *Nat. Nanotechnol.* **4**, 732–737 (2009).
- Wei, J., Wang, Z. H., Chen, W. & Cobden, D. H. New aspects of the metal-insulator transition in single-domain vanadium dioxide nanobeams. *Nat. Nanotechnol.* **4**, 420–424 (2009).
- Liu, W. T. *et al.* Intrinsic Optical Properties of Vanadium Dioxide near the Insulator-Metal Transition. *Nano Lett.* **11**, 466–470 (2010).
- Driscoll, T. *et al.* Memory Metamaterials. *Science* **325**, 1518–1521 (2009).
- Hu, B. *et al.* External-Strain Induced Insulating Phase Transition in  $\text{VO}_2$  Nanobeam and Its Application as Flexible Strain Sensor. *Adv. Mater.* **22**, 5134–5139 (2010).
- Shibuya, K., Kawasaki, M. & Tokura, Y. Metal-insulator transition in epitaxial  $\text{V}_{1-x}\text{W}_x\text{O}_2$  ( $0 < x < 0.33$ ) thin films. *Appl. Phys. Lett.* **96** (2010).
- Wu, T. L., Whittaker, L., Banerjee, S. & Sambandamurthy, G. Temperature and voltage driven tunable metal-insulator transition in individual  $\text{W}_x\text{V}_{1-x}\text{O}_2$  nanowires. *Phys. Rev. B* **83**, 073101 (2011).
- Gu, Q., Falk, A., Wu, J. Q., Lian, O. Y. & Park, H. Current-driven phase oscillation and domain-wall propagation in  $\text{W}_x\text{V}_{1-x}\text{O}_2$  nanobeams. *Nano Lett.* **7**, 363–366 (2007).
- Whittaker, L., Wu, T. L., Patridge, C. J., Sambandamurthy, G. & Banerjee, S. Distinctive finite size effects on the phase diagram and metal-insulator transitions of tungsten-doped vanadium(iv) oxide. *J. Mater. Chem.* **21**, 5580 (2011).
- Tang, C. *et al.* Local atomic and electronic arrangements in  $\text{W}_x\text{V}_{1-x}\text{O}_2$ . *Phys. Rev. B* **31**, 1000–1011 (1985).
- Booth, J. M. & Casey, P. Anisotropic Structure Deformation in the  $\text{VO}_2$  Metal-Insulator Transition. *Phys. Rev. Lett.* **103**, 086402 (2009).
- Di Cicco, A. *et al.* Interplay between morphology and metallization in amorphous-amorphous transitions. *Phys. Rev. B* **78**, 033309 (2008).
- Yao, T. *et al.* Understanding the Nature of the Kinetic Process in a  $\text{VO}_2$  Metal-Insulator Transition. *Phys. Rev. Lett.* **105**, 226405 (2010).
- Sohn, J. I. *et al.* Surface-Stress-Induced Mott Transition and Nature of Associated Spatial Phase Transition in Single Crystalline  $\text{VO}_2$  Nanowires. *Nano Lett.* **9**, 3392–3397 (2009).
- Holman, K. *et al.* Insulator to correlated metal transition in  $\text{V}_{1-x}\text{Mo}_x\text{O}_2$ . *Phys. Rev. B* **79**, 245114 (2009).
- Guo, H. *et al.* Mechanics and Dynamics of the Strain-Induced M1-M2 Structural Phase Transition in Individual  $\text{VO}_2$  Nanowires. *Nano Lett.* **11**, 3207–3213 (2011).
- Whittaker, L., Patridge, C. J. & Banerjee, S. Microscopic and Nanoscale Perspective of the Metal-Insulator Phase Transitions of  $\text{VO}_2$ : Some New Twists to an Old Tale. *J. Phys. Chem. Lett.* **2**, 745–758 (2011).
- Marini, C. *et al.* Optical properties of  $\text{V}_{1-x}\text{Cr}_x\text{O}_2$  compounds under high pressure. *Phys. Rev. B* **77**, 235111 (2008).

- Pouget, J. P. *et al.* Dimerization of a linear Heisenberg chain in the insulating phases of  $\text{V}_{1-x}\text{Cr}_x\text{O}_2$ . *Phys. Rev. B* **10**, 1801–1815 (1974).
- Pouget, J. P., Launois, H., D'Haenens, J. P., Merenda, P. & Rice, T. M. Electron Localization Induced by Uniaxial Stress in Pure  $\text{VO}_2$ . *Phys. Rev. Lett.* **35**, 873–875 (1975).
- Strelcov, E., Davydov, A. V., Lanke, U., Watts, C. & Kolmakov, A. In Situ Monitoring of the Growth, Intermediate Phase Transformations and Templating of Single Crystal  $\text{VO}_2$  Nanowires and Nanoplatelets. *ACS nano* **5**, 3373–3384 (2011).
- Patridge, C. J., Whittaker, L., Ravel, B. & Banerjee, S. Elucidating the Influence of Local Structure Perturbations on the Metal-Insulator Transitions of  $\text{V}_{1-x}\text{Mo}_x\text{O}_2$  Nanowires: Mechanistic Insights from an X-ray Absorption Spectroscopy Study. *J. Phys. Chem. C* **116**, 3728–3736 (2012).
- Netsianda, M., Ngoepe, P. E., Richard, C., Catlow, A. & Woodley, S. M. The displacive phase transition of vanadium dioxide and the effect of doping with tungsten. *Chem. Mater.* **20**, 1764–1772 (2008).
- Kresse, G. & Joubert, D. From ultrasoft pseudopotentials to the projector augmented-wave method. *Phys. Rev. B* **59**, 1758–1775 (1999).
- Dudarev, S. L., Botton, G. A., Savrasov, S. Y., Humphreys, C. J. & Sutton, A. P. Electron-energy-loss spectra and the structural stability of nickel oxide: An LSDA+U study. *Phys. Rev. B* **57**, 1505–1509 (1998).
- Kubler, C. *et al.* Coherent structural dynamics and electronic correlations during an ultrafast insulator-to-metal phase transition in  $\text{VO}_2$ . *Phys. Rev. Lett.* **99**, 116401 (2007).
- Hilton, D. *et al.* Enhanced Photosusceptibility near  $T_C$  for the Light-Induced Insulator-to-Metal Phase Transition in Vanadium Dioxide. *Phys. Rev. Lett.* **99**, 226401 (2007).
- Arcangeletti, E. *et al.* Evidence of a Pressure-Induced Metallization Process in Monoclinic  $\text{VO}_2$ . *Phys. Rev. Lett.* **98**, 196406 (2007).
- Qazilbash, M. M. *et al.* Mott transition in  $\text{VO}_2$  revealed by infrared spectroscopy and nano-imaging. *Science* **318**, 1750–1753 (2007).
- Ravel, B. & Newville, M. ATHENA, ARTEMIS, HEPHAESTUS: data analysis for X-ray absorption spectroscopy using IFEFFIT. *J. Synchrotron Rad.* **12**, 537–541 (2005).
- Newville, M. IFEFFIT: interactive XAFS analysis and FEFF fitting. *J. Synchrotron Rad.* **8**, 322–324 (2001).
- Zhong, W. J. & Wei, S. Q. USTCXAFS 2.0 Software Packages. *J. Univ. Sci. Technol. China* **31**, 328–333 (2001).

## Acknowledgements

This work is financially supported by the National Basic Research Program of China (No. 2009CB939901), the National Natural Science Foundation of China (Grant Nos. 11135008, 11079004, 10979044), the Knowledge innovation project of the Chinese Academy of Sciences (KJCX2-YW-N40), and Shanghai Key Basic Research Project (3109DJ1400201).

## Author contributions

X.G.T. and T.Y. contributed equally to this work, performed the experiments, collected and analyzed the data, and wrote the paper; R.L., X.G.T. and C.Z.W. synthesized the samples; T.Y., Y.J.F. and H.C. performed XAFS experiments; Z.H.S. helped with data analysis; X.Y., W.Q.Z. and Q.H.L. performed theoretical calculations; Y.X. and S.Q.W. conceived the experiments, analyzed results, and wrote the paper.

## Additional information

**Competing financial interests:** The authors declare no competing financial interests.

**License:** This work is licensed under a Creative Commons Attribution-NonCommercial-ShareAlike 3.0 Unported License. To view a copy of this license, visit <http://creativecommons.org/licenses/by-nc-sa/3.0/>

**How to cite this article:** Tan, X. *et al.* Unraveling Metal-insulator Transition Mechanism of  $\text{VO}_2$  Triggered by Tungsten Doping. *Sci. Rep.* **2**, 466; DOI:10.1038/srep00466 (2012).